FULL-SCALE TESTING AND NUMERICAL ANALYSIS OF A PRECAST FIBRE REINFORCED SELF-COMPACTING CONCRETE SLAB PRE-STRESSED WITH BASALT FIBRE REINFORCED POLYMER BARS

BRUNO DAL LAGO[1*], SU E. TAYLOR[2], PETER DEEGAN[3], LIBERATO FERRARA[1], MOHAMMED SONEBI[2], PHILIP CROSSET[2], and ANDREA PATTARINI[4]

[1] Department of Civil and Environmental Engineering, Politecnico di Milano, p.za Leonardo da Vinci 32, 20133 Milano, Italy

[2] School of Natural and Built Environment, Queen's University, University Road, BT7 1NN Belfast, Northern Ireland, UK

[3] Banagher Precast Concrete, Queen Street, Banagher, Republic of Ireland

[4] Azichem, via Gentile 16a, Goito (MN), Italy

* Corresponding author: brunoalberto.dallago@polimi.it

Abstract

Steel-free pre-stressed reinforced concrete may be used in aggressive environments to increase the durability of structural elements and to limit the carbon footprint by replacing steel with high-strength fibre composites. The design of a 10-m long steel-free precast fibre-reinforced concrete slab, pre-stressed with basalt-fibre reinforced polymer (BFRP) bars and shear-reinforced with glass-fibre reinforced polymer bars, is presented in this paper. Non-linear viscoelastic and elastic-plastic models have been employed for the prediction of the service and ultimate limit state flexural behaviour, respectively. Preliminary tests on the employed materials and a 3-point load test on the slab element are presented, together with indications on its manufacturing process. The proposed numerical analysis is validated against the experimental results.

Keywords: Steel-Free beams; Fibre Reinforced Self-Compacting Concrete (FRSCC); Basalt Fibre Reinforced Polymer (BFRP) Bars; Creep Losses; Visco-Elastic Analysis; Non-Linear Analysis.

1. Introduction

The use of composites in structural applications is constantly increasing with the aim of providing adequate responses to the worldwide challenges of durability and reduction of CO_2 emissions. Basalt fibre reinforced polymers (BFRP) are advanced composite materials, and extensive research activity has been devoted to their production and possible applications in different fields of engineering, including civil engineering (Fiore et al. [1]). The use of BFRP bars in concrete structural elements was investigated by Tharmarajah et al. [2], Zhang et al. [3], High et al. [4], Elgabbas et al. [5], Fan & Chang [6,7] and applied with self-compacting concrete (SCC) in Thompson's bridge in Northern Ireland (Taylor et al. [8]).

BFRP bars are characterised by a high rupture strength, ranging from 920 to 1650 MPa, and a relatively low elastic modulus, ranging from 45 to 59 GPa (Crossett et al. [9]). These particular features make their application in pre-stressed concrete promising, since their resistance may be comparable with that of traditional pre-stressing steel, while having an elastic modulus about four times smaller. This implies that both elastic and long-term pre-stressing losses occurring in pre-stressed concrete elements due to the shortening of the member could be relevantly reduced. Composite reinforcement as a pre-stressing material was investigated by Nanni and Tanigaki [10], Leung et al. [11], Lees and Burgoyne [12] (aramid), Stoll et al. [13] and Du et al. [14] (carbon), Atutis et al. [15] (glass) and Crossett et al. [9] (basalt). Zheng et al. [16] and Li et al. [17] studied the application of carbon composite bars as unbonded external post-tensioning reinforcement in concrete structures, whereas their application to post-tension timber structural elements was experimentally investigated by McConnell et al. [18]. BFRP bars, like all fibre composite materials, are characterised by an orthotropic mechanical behaviour, with a better performance when the load is applied in the direction of the fibres, while the strength is typically much lower when the load is applied orthogonally with respect to the fibres. This makes BFRP bars more vulnerable in the area of the anchorage, where, because of wedge devices typically used for steel tendons, strong lateral pressures are likely to be applied. Alternative technological solutions to be applied to fibre composite bars were proposed by Reda Taha and Shrine [19], Al-Mayah et al. [20], Carvelli et al. [21], Schmidt et al. [22] and Crosset et al. [9]. The transfer length of composite pre-stressing reinforcement was investigated by Ehsani et al. [23] (aramid and carbon), Soudki et al. [24], Mahmoud et al. [25] and Lu et al. [26] (carbon), Fava et al. [27] and Yan et a. [28] (glass) and Crosset et al. [29] (basalt).

The design procedures under serviceability and ultimate limit states for pre-stressed concrete elements using BFRP bars are not codified yet, even if general information related to FRP reinforcement in concrete is available in ACI 440.1R-15 [30]. Bischoff [31] provided a comparison among different methodologies used to estimate deflection in concrete elements reinforced with steel or FRP bars. Zou [32], Youakim and Karbhari [33] and Zou and Shang [34] proposed a simplified methodology to evaluate the pre-stressing losses in service and the deflection of beams pre-stressed with composite bars. Dolan et al. [35] provided information about simplified formulations to estimate the strength of concrete sections pre-stressed with FRP, while Knight et al. [36] proposed a more sophisticated segmental approach. Pisani [37,38] and Lou et al. [39] studied the long-term behaviour of concrete beams pre-stressed with aramid tendons.

The paper presents the results of a full-scale test on a steel-free precast slab made of fibre-reinforced SCC pre-stressed with BFRP bars. A semi-analytical procedure based on a sectional approach for the evaluation of serviceability and ultimate limit state flexural behaviour of concrete elements pre-stressed with BFRP bars is proposed in the paper, whose predictions are validated through the comparison with the experimental results. A similar procedure for precast concrete pre-stressed with steel tendons was reported by Dal Lago et al. [40].

Previous research [9,41] has outlined the tests on the concrete materials including the mix optimisation with and without fibres and the residual flexural strength with different fibre volumes.

2. Experimental set-up

A hollow light-weight 10 m long slab element was considered for this industrial led research. The cross section, shown in Figure 1, is not symmetrical along the vertical axis. The edge corbels enable the dowel connections between adjacent elements and is typical of pre-cast slab technology employed in Ireland and the UK. The positioning of the pre-stressing BFRP bars was studied in such a way to minimise the torsional effects. The element was designed to be used as a roof element, for which the additional dead loads (other than self-weight), waterproofing and thermal insulation layers, may be considered negligible. The only design condition adopted, without a reference to a snow load, refers to the serviceability limit state, with the aim of providing a stable evolution of the camber, similarly to what is widely adopted in the design of traditional pre-stressed members with steel tendons. This means that the member will have a

pre-camber and not a downward deflection after pre-stressing release, but it also maintains a controlled camber over time.

12-mm diameter (Φ12) BFRP bars, with a 40-mm cover to the soffit for a full stress distribution in the concrete, were used as the pre-stressing reinforcement and were designed to be pre-stressed to 500 MPa, which corresponds to about half of their ultimate rupture strength as measured in laboratory tests at Queen's University Belfast. Two shear resisting trusses made of inclined 6-mm diameter GFRP bars were also inserted in the element, one in correspondence of each rib.

3. Materials

3.1 Basalt Fibre Reinforced Polymer (BFRP) bars

The behaviour of the Φ12 BFRP bars was investigated by means of tensile tests at the Queen's University of Belfast and at Politecnico di Milano. Figure 2(a) shows the test setup; the detail of the anchorage, made with carborundum-aluminium sheets, is presented in Figure 2(b). A loading rate of 0.2 kN/s was used in all tests. A perfectly elastic behaviour was observed for all bars up to failure. A mean elastic modulus of 48 GPa was consistently obtained with negligible standard variation.

In regard to the bar strength, the failure was influenced by the anchorage. A picture of one broken bar is reported in Figure 2(c). After removal of the bar from the mechanical wedges, it could be observed that the bar ends clamped by the wedges were highly deformed (Figure 2d), which suggests that they contributed to the failure. The ultimate strength attained in the tests varies in the range 600~800 MPa. According to the supplier information, their rupture strength is of 1000 MPa, which corresponds to an ultimate strain of about 2%. However, previous research [42] shows how the rupture strength can increase significantly with the loading rate and, therefore, the definition of this structural property should always be related to the loading rate used.

The transfer length of the bars was monitored through experimental testing of small beam specimens at Queen's University of Belfast. Figure 3 shows the experimental setup. The results are presented in detail together with analytical considerations in Crosset et al. [29] and indicate that the Φ12 sand coated BFRP bars pre-stressed at 450 MPa were fully anchored to within a 10-diameters length, which points out the efficiency of the sand coated surface treatment of the bars in enhancing their bond with concrete.

A long-term tensile test was carried out in a controlled environment (T = 20 °C; RH = 60%) chamber at Politecnico di Milano with the aim of investigating the relaxation behaviour of one Φ12 BFRP bar pre-stressed at 500 MPa over 60 days (the ageing time of the tested beam). Pictures of the setup are shown in Figure 4. The results, plotted in Figures 5a and 5b, with a loss percentage over 1000 h ρ_{1000} equal to 8.4% and a loss over two months equal to 9.4%, indicate that BFRP bars are experiencing high relaxation losses, even if pre-stressed to about half of their strength. The classical formulation of relaxation losses for pre-stressing steel (Equation 1) reported in the Eurocode 2 [43] was fitted against the experimental BFRP curve by calibrating the parameters k and μ.

$$\frac{\Delta\sigma_{pr}}{\sigma_{pi}} = \text{k}\rho_{1000}e^{9.1\mu}\left(\frac{t}{1000}\right)^{0.75(1-\mu)}10^{-5} \tag{1}$$

Two curves were obtained (Figure 5c), the first with $k = 2.1$ and $\mu = 0.74$ matches with precision the experimental trend up to about 900 hours (lower bound); the second with $k = 2.9$ and $\mu = 0.72$ matches quite precisely the trend at a longer time (upper bound). The lower bound curve is suggested as the most realistic, since the experimental relaxation curve seems to have a "lay-out" stress shift after 900 hours which might have depended on a very small sliding at the anchorages.

3.2 Fibre-Reinforced Self-Compacting Concrete (FRSCC)

Table 1 summarises the mix composition of the employed Fibre-Reinforced Self-Compacting Concrete (FRSCC) which was developed from previous laboratory tests (Garcia-Taengua et al. [41]). The mix features a water-to-binder (w/b) ratio of 0.45 with a polycarboxylate superplasticiser (SP), which provided adequate flowability (slump flow diameter 700 mm, Jring height difference 18 mm) and viscosity (V-funnel time 20 s) also in presence of fibres (38-mm long polypropylene -PP- fibres were employed). In order to improve the sustainability of the mix, part of the cement was replaced with ground granulated blast furnace slag (GGBS); limestone powder (LSP) was also employed as fine. A self-healing admixture (SH) was added to the mix for research purposes which are out of the subject of the present paper (see [44,45] for details on the topic).

3.3 Glass Fibre Reinforced Polymer (GFRP) bars

GFRP bars were used as shear reinforcement. GFRP bars are a more standard and established structural product in comparison with BFRP bars. The supplier reported a rupture strength of 900 MPa and an elastic modulus of 46 GPa. Previous research by Tharmarajah [42] shows a comparison of GFRP and BFRP.

4. Manufacturing

The slab element was cast at the Banagher Concrete Ltd factory in Banagher, Co. Offaly, Ireland. The whole process is illustrated in the following section, highlighting the challenges that occurred, as also discussed in Dal Lago et al. [46]. The element was cast on a longer pre-stressing bed. Thus, an inner timber mould was built (Figure 6a) as the stop end for the 10-m slab. The BFRP bars had been ordered with a length of 12 m, which was too short for the 15-m bed. To overcome this, steel couplers were applied externally with respect to the inner mould (Figure 6b) and coupled bars gave an overall length of 18 m to accommodate the hydraulic jack for pre-stressing and enable anchoring which was carried out using traditional steel tendons wedges on the opposite side.

Traditional wedges used for pre-stressing steel were chosen despite the literature suggesting the low efficiency of this clamping mechanism due to the strong concentration of transversal stress in the bars. However, the literature mainly refers to the testing equipment associated with the rupture of the bar while in this study the temporary restraint was for a pre-stress level of 50% of the rupture strength and several trials performed at the factory were positive in terms of applying the pre-stress. Optical sensors were installed prior to tensioning at positions calculated taking into account the expected elongation of the bars (based on the measured elastic modulus at a loading rate of 0.2 kN/s) to monitor the transfer length at both the loaded end and the dead end (or opposite end to where the pre-stress is applied).

The BFRP bars were stressed with a hollow core hydraulic jack with an automatic wedge pushing system, the same as the one used for steel tendons. Figure 6(c) shows Peter Deegan, Director at Banagher Ltd, stressing each of the bars, which were pulled from the same side with an initial stress of 500 MPa. This corresponded to a load of 56.5 kN, and a total elongation of 155 mm over the length of the mould (15 m). The operation was successful and the elongation was checked for each cable and was as predicted. After about 15 minutes from stressing, the first tensile failure of one bar occurred in correspondence of the

wedge, due to the lateral pressure exerted by it causing an initial failure in the outer fibres and then subsequently the inner fibres which were carrying the full load. Within the following 30 minutes, two additional similar failures occurred. Figure 7 shows one bar after failure at the anchorage zone.

The first failed bar was removed and replaced with a new bar, which, for safety reasons, was not pre-tensioned. It appears that the failure was a result of the detail at the wedges as this was not used in the laboratory tests where a protective coat of epoxy resin was used between the bar and the wedges as outlined in Crossett et al [9] . It was decided to continue with the casting of the FRSCC, and accepting the loss of two pre-stressing bars and the failed stressing of one of them. Since removing of the failed bars was judged to be unsafe, they were left in the mould.

The concrete casting was successfully performed with the concrete flowing under its own self weight and uniform dispersion of fibres was obtained except for a very few isolated clots which were removed by hand or with a rake.

After having poured the lower flange, the shear resisting trusses were inserted into the corresponding ribs (Figure 6d). Afterwards, the polystyrene blocks were inserted and the ribs and the upper flange were then cast. No additional issues were experienced in the phases of pre-stressing release and curing.

The pre-stress was released after three days from casting. The slab element was stored indoors for three weeks from casting, and then outdoors for six weeks until the day of the test.

5. Prediction of performance in service

Due to the use of an innovative material in the slab, the simplified formulation for the estimation of pre-stressing losses provided by Eurocode 2 [43], based on the linearisation of the long-term interaction among the phenomena influencing deformability, including viscoelastic member shortening, concrete shrinkage and reinforcement relaxation, was not used. A new analytical procedure based on the explicit interaction which decouples the longitudinal and transversal deformation, whilst taking into account the shortening evolution profile to assess the pre-stressing losses, was used (Dal Lago et al. [47]).

The deflection profile of the member was calculated in accordance with a viscoelastic model having the following integral form:

$$v(t, t_0) = v_e(t) + \int_{t_0}^{t} v_e(t)\dot{\varphi}(t, t_o)dt \tag{2}$$

where the viscoelastic transversal deflection v at time t is expressed as the sum of the contribution of the elastic deformation computed at time t and of the contribution of creep, depending on the first derivative of the creep coefficient $\varphi(t,t_0)$.

With reference to the behaviour of pre-stressed elements during the storage phase, the elastic contribution always has a monotonic decreasing trend, due to the combination of the following phenomena:

- stiffening over time due to the ageing of the concrete,

- viscoelastic shortening of the member and subsequent elastic losses in the bars,

- relaxation of the pre-stressing reinforcement,

- shrinkage of concrete.

The creep contribution, if the elastic component is always positive and characterised by a monotonic increasing trend.

The combination of these terms gives the overall deformation behaviour of the element, which could also be subjected to a reversal of the deflection trend in the range of upwards values. This cannot be described in mathematical terms without a precise evaluation of the member shortening evolution with time.

The employed methodology solves the problem by means of numerical techniques through a discretisation in the time domain, under the assumption of section strain profile remaining plane and homogeneous section. In particular, the longitudinal and transverse behaviour of the element are considered as uncoupled, and the formulation is corrected with linear terms in order to take into account, in a simplified way, the real coupling. As a consequence of such a hypothesis, it is possible to formulate the calculation of the longitudinal shortening, and subsequently compute the transverse deformation history as a function of the thus determined shortening evolution.

The longitudinal strain may be written as follows, depending on the elastic, creep and shrinkage strains:

$$\varepsilon_{long}(\bar{t}, t_0) = \varepsilon_{el}(\bar{t}, t_0) + \varepsilon_{creep}(\bar{t}, t_0) + \varepsilon_{cs}(\bar{t}) \tag{3}$$

with

$$\varepsilon_{creep}(\bar{t}, t_0) = \int_{t_0}^{\bar{t}} \varepsilon_{el}(t)\dot{\varphi}(t, t_o)dt \tag{4}$$

$$\varepsilon_{el}(\bar{t}, t_0) = \frac{\sigma_p(\bar{t},t_0)A_p}{E_{cmj}(\bar{t})A_c} \Phi_{anch} \tag{5}$$

The mean stress $\sigma_p(t,t_0)$ in the pre-stressing reinforcement can be defined as follows, taking into account the losses for relaxation, thermal deformation and shortening:

$$\sigma_p(\bar{t}, t_0) = \sigma_{p0}\left(1 - \Phi_\chi A_p \frac{z_{cp}^2}{I_{id}}\right) - \Delta\sigma_{pr}(\bar{t}) - \frac{\Delta P_\theta}{A_p} - \varepsilon_{long}(\bar{t}, t_0)E_p A_p \tag{6}$$

where an anchorage factor Φ_{anch} is simply defined in average terms for the distribution of end short debonding ducts and anchorage of the pre-stressing reinforcement as follows:

$$\Phi_{anch} = \frac{\Sigma_p\left(L - L_{anch,p}\frac{\sigma_{p0,p}}{mean(\sigma_{p0})}\right)}{Ln_p} \tag{7}$$

Φ_χ is a weighted factor for curvature loss taking into account the combination of parabolic-shaped deformation profile due to pre-stressing and fourth order polynomial function deformation profile due to distributed loads (self-weight), to which the maximum bending M' and $M*$, respectively, correspond. The Φ_χ factor is always lower than one.

$$\varphi_\chi = \frac{v_{max,p}}{v_{max,q+p}} = \frac{M'L^2}{8EI} \Bigg/ \left(\frac{5M*L^2}{48EI} + \frac{M'L^2}{8EI}\right) = \left(1 + \frac{5}{6}\frac{M*}{M'}\right)^{-1} \tag{8}$$

The non-linearity of Equation 3 is evident, due to the presence of the unknown longitudinal strain ε_{long} in the integral. The solution cannot be obtained in closed form, and the equation has to be solved with the aid of numerical techniques. An approximated solution with independent variables can anyway be identified by estimating the loss for shortening of the member, through a fictitious stiffening of the axial deformability. Such a simplification, after having introduced proper correction terms, introduces negligible errors.

Considering the basic material properties of strength development, shrinkage and creep of concrete recommended in the Eurocode 2 [43], the deflection profile of the slab, shown in Figure 8 at pre-stressing release and after 58 days of curing, is practically stable around the perfect straightness, as also shown in Figure 9 by the mid-span camber vs time diagram. The contribution of the slab self-weight is considered in both diagrams. Figure 9 also shows the evolution of shortening over time. Positive values indicate shortening and camber. The deflection profiles plotted in Figure 8 are deduced from the sum of the parabolic-shaped contribution of pre-stressing and the fourth order polynomial function due to the self-weight of the beam. The global mean pre-stressing losses obtained were 2.3% due to viscoelastic shortening (including shrinkage) plus 10.3% due to relaxation, for a total of 12.6%.

It is worth noting that sample measurements on the case study slab confirm the order of magnitude of the predictions.

6. Prediction of performance up to failure

A section approach was considered for the evaluation of the flexural behaviour of the slab element. The employed analytical procedure starts with the definition of the sectional geometry and the material properties, evaluating the bending moment vs curvature diagram of the section by applying force and moment equilibria. Pre-stressing is taken into account by including the initial strain ε_i of the n_r reinforcing elements in the Equations (9).

$$N = \int_0^h \sigma_c(\varepsilon)b(y)dy + \sum_{n=1}^{n_r} \sigma_r(\varepsilon + \overline{\varepsilon_i})A_{r,n} \tag{9}$$

$$M = \int_0^h \sigma_c(\varepsilon)b(y)(y - y_G)dy + \sum_{n=1}^{n_r} \sigma_r(\varepsilon + \overline{\varepsilon_i})(\overline{y_n} - y_G)A_{r,n}$$

Given the material stress vs strain curves, the problem is governed by the external actions *N, M* and by the sectional strain distribution, function of two parameters, for example the angle of curvature χ and the strain of the top fibre ε_{sup}. Two unknowns can be calculated by solving the equations. For pre-stressed beams, usually there is no external axial load: N = 0. For a curvature control calculation, a given sectional curvature angle χ can be imposed, evaluating from equations (9) the upper strain ε_{sup} and the bending moment *M*. For a moment control calculation, a given bending moment *M* can be imposed, evaluating from equations (9) the upper strain ε_{sup} and the curvature angle χ.

The solution of these equations for a set of curvature or moment values yields a bending moment vs curvature diagram. Starting from this diagram, the non-linear deflection profile of the beam can be evaluated by integrating twice the curvature along the slab element and imposing the boundary conditions. To perform this operation, a moment control diagram is preferable, since it always provides an injective function. For statically determinate beams, where redistribution of moments does not occur, and thus the moment distribution is always known, the use of moment or curvature control diagrams yields to the same results.

This procedure has been applied to the case study slab above described. Figure 10(a) shows the stress-strain relationship for concrete, evaluated based on the modified Sargin compression model proposed in Model Code 2010 [48] for a class C70/85 concrete. High strength was considered here based upon the average results of compressive strength tests carried out on cube concrete specimens on the day of the first structural test. A tensile linear behaviour was adopted up to the average tensile strength, calculated as per Eurocode 2 [43], with a softening post-peak behaviour down to a tensile residual concrete strength

equal to 0.51 MPa, which is due to the polypropylene fibres. Such a value was calculated from residual experimentally measured strength values of the employed FRSCC mix, tested as per EN-14651 [49] and according to Model Code 2010 [48] (Garcia-Taengua et al. [50]). The tensile behaviour of BFRP was modelled through an elastic relationship with elastic modulus equal to 48 GPa and an ultimate strength of 1000 MPa (Figure 10b).

Figure 11 shows the non-linear bending moment vs curvature diagrams obtained adopting a curvature- or a bending moment-controlled procedure. After a stiff elastic phase, cracking is expected to occur at about 315 kNm, followed by a loss of strength due to cracking.

A post-cracking softer linear phase stabilises on the basis of the elastic deformation of the BFRP bars in tension up to failure of the pre-stressed bars only at about 400 kNm. The residual strength of about 90 kNm is due to the non-stressed bars, that are at about half of their elongation capacity (0.96%) and to the contribution of polypropylene fibres. At post-failure curvature increase, the non-pre-stressed bars fail after a relevant additional curvature increase, with a residual bending moment equal to 32 kNm which is due to the constant post-cracking contribution of the polypropylene fibres.

7. Parametric analysis

A parametric investigation was carried out with the aim of comparing the effect of pre-stressing on the flexural behaviour of a beam pre-stressed with BFRP bars or traditional high resistance steel tendons. The case study slab element was selected as a benchmark, and the two types of reinforcement were designed to attain a similar flexural strength. Twelve BFRP bars with 12 mm of diameter and 7 tendons with 12.7 mm (0.5") of diameter, both provided with a 40-mm cover from the soffit were considered. The stress vs strain relationship for class C45/55 concrete was evaluated in accordance with what previously described, considering its tensile strength and neglecting the contribution of the fibres. The BFRP bars were modelled as described above. The pre-stressing steel was modelled with an elastic-plastic relationship considering an elastic modulus of 195 GPa, a yield strength $f_{p0.1k}$ equal to 0.9 f_{pk}, an ultimate strength f_{pk} equal to 1860 MPa and a linear hardening branch from yield to failure at an ultimate strain of 6%.

Figure 12 shows the non-linear bending moment vs curvature diagrams for the two reinforcement options considering an increasing pre-stressing as a percentage of the ultimate strength for BFRP bars and of the yield strength for steel tendons. A dimensionless bending moment is indicated on the vertical axis; it has

been calculated as the ratio between the computed and the ultimate moment for BFRP reinforcement calculated as $M_{rd} = 0.9 \, d \, A_r \, f_u$ and between the computed and the yield moment for steel reinforcement calculated as $M_{rd} = 0.9 \, d \, A_r \, f_{p0.1k}$, where d is the sectional effective depth.

For both reinforcement types, a higher initial pre-stress corresponds to a higher cracking moment, providing an enhanced service performance. For both reinforcements, the ultimate strength is not affected by the pre-stressing, as expectable when the failure is on the tensioned side. For BFRP reinforcement, this is only valid if the bars are placed at the same depth and are all pre-stressed at the same level. Elsewise, they will not attain failure at the same time, and the reinforcement will not be fully exploited (see Figure 11). Conversely, when the failure occurs for concrete crushing with elastic reinforcement, the ultimate strength increases with the pre-stressing, as confirmed by the experimental tests described in [9].

The post-cracking behaviour of the slab reinforced with BFRP is elastic up to failure, which occurs due to a brittle tensile failure of the bars. Since the post-cracking residual elongation of the bars depends on the level of pre-stress, it highly affects the deformation capacity of the section. The higher the pre-stressing, the lower the deformation capacity. The steel tendons exhibited elastic-plastic behaviour, and failure occurred due to crushing of concrete after the development of plastic strain in the reinforcement, which largely overcame the elastic deformation due to pre-stress. Therefore, the deformation capacity was not as affected by the pre-stressing compared to BFRP.

8. Test results and comparison with predictions

The case study slab element (shown in Figure 13 after demoulding) was subjected to a 3-point bending test applied using an accurately calibrated 50t capacity hydraulic ram positioned at mid-span with +300 mm stroke mono-directional and counter-acting on a steel reaction frame. Figure 14 shows the test rig. The slab was simply supported at the edges on stiff concrete blocks. 10 mm thick timber slats were placed between the element and the supporting blocks to distribute the load. The load was applied at mid-span and a load cell was installed on the external hydraulic pump to measure the applied load. A steel box beam was placed between the jack and the slab for equal load distribution. Three digital displacement transducers (LVDTs) were placed at the soffit of the mid-span section, one at the centre and two near the beam side face edges. Two additional dial gauges were placed at about 560 mm from the support to

measure any settlement at the support region. The load was applied incrementally and in cycles (Figure 15).

The experimental results are plotted in Figure 16 in terms of applied point load vs mid-span deflection. They highlight an elastic behaviour up to cracking, at an applied load of ~70 kN, after which the behaviour stabilises on a softer elastic curve also featuring a progressive cyclic stiffness degradation due to the diffusion of cracks from mid-span towards the ends. The stiffness lowered by about 5 times, from 16.3 kN/mm of the pre-cracking stage to 3.2 kN/mm after the post-cracking stage at large deflections. The test was performed up to a load of 155 kN, and it was stopped when the load started to become unstable. . The displacement data from the last load cycle was not recorded as the transducers were removed for the safety reasons. An approximate deflection of 190 mm was attained as an estimation from the image data recorded with a camera mounted on a fixed tripod. Further work is ongoing to establish deflections, curvature and rotations from the image data [51].

The large deflection of the slab at the 120 kN applied load cycle is observable in Figure 17. An efficient recovery of the deflection was observed after each load step prior to the end (up to 120 kN). The crack pattern at the 120 kN cycle is shown in Figure 18. The numbers indicate the pressure level of the pump in bars at the formation of the crack. A factor of 2.33 kN/bar was calibrated to convert bars into an applied load in kN. The crack pattern evolution with load is sketched in Figure 19 and the failure crack is highlighted in red.

A good distribution of cracks equated to small crack openings. The formation of the cracks at each location typically occurred with a vertical major one with smaller adjacent cracks forming at a space equal to the fibre length and converging towards the vertical one. Polypropylene fibres strongly contributed to the distribution of the cracks. The mid-span cracks propagated up to about 50 mm from the slab extrados, inclining towards the point load in the upper branch due to the shear action. Inclined shear cracks near the supports were not observed. After unloading at all load cycle amplitudes, all cracks closed due to the pre-stressing action.

The numerical curve obtained from the above described procedure is also plotted in Figure 16 omitting the contribution of the distributed dead load from the structural weight of the slab, thus allowing for a direct comparison with the experimental results. The elastic stiffness matches the experimental one with remarkable agreement. The crack load is slightly over-estimated at about 90 kN. The experimental crack

value might have been lowered by the cyclic increase of the load, as well as by some pre-existing shrinkage-induced diffused micro-cracks. The numerical post cracking softer elastic stiffness also matches the experimental one. The predicted ultimate curvature is attained at the mid-span at a load of 150 kN, which corresponded to the tensile failure of the BFRP pre-stressed bars. The slightly higher maximum experimental load compared to the predictions is probably due to a rupture strength of the BFRP bars higher than 1000 MPa and/or to a better contribution of fibres which may have aligned along the flow of FRSCC in the relatively thin bottom flange. The slab element was re-tested nine months later in order to confirm if the failure mode was for bending. Bending failure was obtained for flexure due to the rupture of the BFRP bars, as expected. The failure crack was located at about 700 mm from mid-span on the North-West side. At complete failure, after the load already dropped significantly, the upper concrete layer of the slab failed with an additional inclined crack that started from the main vertical one. This was due to the influence of shear, since a compressive failure of concrete is to be excluded by observing the failure mode. Figure 20 shows pictures of the slab after failure. The detailed picture in Figure 20(c) shows a BFRP bar failed in tension, while the detailed picture in Figure 20(d) shows an intact GFRP bar of the shear-resisting truss.

9. Conclusions

Design, manufacturing and testing of a 10-m long steel-free precast fibre-reinforced SCC slab pre-stressed with BFRP longitudinal bars and reinforced with GFRP shear-resisting bars has been described in this paper, and the research has demonstrated a novel technological solution for developing corrosion resistant low carbon footprint lower weight precast concrete elements.

The proposed analytical procedure for the estimation of the element's flexural behaviour at both serviceability and ultimate limit states has been presented and successfully implemented.

The mechanical properties of the BFRP bars, their relaxation behaviour and their transfer length in the concrete have been assessed through experimental testing. The results that (1) the elastic modulus was stable and consistent, (2) they are subjected to non-negligible long-term relaxation and (3) the sandblasting surface treatment of the bars is efficient in providing a short transfer length which equates to lower losses.

Despite positive preliminary testing, during element casting, traditional wedge anchorage systems, used for steel, caused some of the bars to fail, due to rupture of the outer fibres even though they were pre-stressed to about half of their strength. This is an issue to be considered for the application of this technology and the resin-based system that was developed for the laboratory tests should be used in future.

The full-scale 3-point load test showed a satisfactory performance of the element, which attained a load larger than the predicted load, corresponding to large mid-span deflections of ~1/50 of the span at peak load. Efficient elastic recovery with low residual deflection and crack closing were observed after unloading at up to 80% of the ultimate load. The crack pattern of the member showed a very good crack distribution and corresponding low mean crack opening, which is mainly attributable to the use of polypropylene fibres in concrete. Failure occurred due to the tensile rupture of the BFRP longitudinal bars. The shear-resisting trusses consisting of GFRP non-bent bars inclined at 45° behaved satisfactorily during the whole test and prevented a diagonal tension failure due to shear. An additional test on the damaged slab was carried out 9 months later to observe its failure mode, which has been, as predicted, dominated by flexure with tensile failure of the BFRP bars.

The predictions obtained on the basis of the presented analytical procedures showed good agreement with the experimental results. This procedure may be safely used for design purposes.

A parametric study into the effect of the initial pre-stressing on the flexural behaviour of the case study slab highlighted the influence of the initial pre-stress on the serviceability performance as well as on the strength (affected only if the bars are placed at different depths and/or they are pre-stressed at a different level) and curvature deformation capacity (affected, since lower ultimate curvature is associated with higher pre-stressing). The strength would have increased with pre-stressing in case failure would have occurred on the concrete side.

The experimental results confirmed that the proposed technology, employing fully non-metallic reinforcement and relying on the toughening effect of the dispersed fibre reinforcement, is a viable and robust structural solution for durable low-carbon FRSCC pre-stressed beams.

References

1. Fiore V, Scalici T, Di Bella G, Valenza A. A review on basalt fibres and its composites. Comp Part B: Eng 2015;74:74-94.

2. Tharmarajah G, Taylor SE, Robinson D, Cleland DJ. Corrosion resistant fibre reinforced polymer (FRP) reinforcement for bridge deck slabs. In: Proceedings of the Institution of Civil Engineers: Bridge Eng 2015;168(3):208-217.

3. Zhang L, Sun Y, Xiong W. Experimental study on the flexural deflections of concrete beam reinforced with basalt FRP bars. Mat and Struct 2016;48:3279-3293.

4. High C, Seliem HM, El-Safty A, Rizkalla SH. Use of basalt fibers for concrete structures. Constr Build Mat 2015;96:37-46.

5. Elgabbas F, Vincent P, Ahmed EA, Benmokrane B. Experimental testing of basalt-fiber-reinforced polymer bars in concrete beams. Comp Part B: Eng 2016;91:205-218.

6. Fan X, Zhang M. Experimental study on flexural behaviour of inorganic polymer concrete beams reinforced with basalt rebar. Comp Part B: Eng 2016;93:174-183.

7. Fan X, Zhang M. Behaviour of inorganic polymer concrete columns reinforced with basalt FRP bars under eccentric compression: An experimental study. Comp Part B: Eng 2016;104:44-56.

8. Taylor SE, Robinson D, Sonebi M. Basalt-fibre-reinforced polymer reinforcement. Concr 2011;April:48-50.

9. Crossett P, Taylor S, Robinson D, Sonebi M, Garcìa-Taengua E, Deegan P, Ferrara L. The flexural behaviour of SCC beams pre-stressed with BFRP. In: Proceedings of the ACIC-7 Conference. Cambridge, September, 2015. p.62-67.

10. Nanni A, Tanigaki M. Pretensioned Prestressed Concrete Members with Bonded Fiber Reinforced Plastic Tendons: Development and Flexural Bond Lengths (Static). ACI Struct J 1992;89(4):433-441.

11. Leung HY, Balendran RV, Maqsood T, Nadeem A, Rana TM, Tang WC. Fibre reinforced polymer materials for prestressed concrete structure. Struct Surv 2003;21(2):95-101.

12.   Lees JM, Burgoyne CJ. Experimental Study of Influence of Bond on Flexural Behavior of Concrete Beams Pretensioned with Aramid Fiber Reinforced Plastics. ACI Struct J 1999;96(3):377-385.

13. Stoll F, Saliba JE, Casper LE. Experimental study of CFRP-prestressed high-strength concrete bridge beams. Comp Struct 2000;49:191-200.

14. Du X, Zuohu W, Jingbo L. Flexural Capacity of Concrete Beams Prestressed with Carbon Fiber Reinforced Polymer (CFRP) Tendons. Advanced Materials Research 2011;168-170:1353–1362.

15. Atutis M, Valivonis J, Atutis E. Analysis of serviceability limit state of GFRP prestressed concrete beams. Comp Struct 2015;134:450-459.

16. Zheng WZ, Bai CX, Cheng HD. Experimental Study on Behaviors of Unbonded Prestressed Concrete Beams Reinforced with CFRP Tendons. Key Eng Mat 2009;400-402:567-573.

17. Li HF, Gong C, Fang Z. Behaviors of Concrete Beam Prestressed with External CFRP Tendons. Key Eng Mat 2009;400-402:559-566.

18. McConnell E, McPolin D, Taylor S. Post-tensioning glulam timber beams with basalt FRP tendons. Constr Mat 2015;168(5):232-240.

19. Reda Taha M, Shrive NG. New Concrete Anchors for Carbon Fiber-Reinforced Polymer Post-Tensioning Tendons - Part 2: Development/Experimental Investigation. ACI Struct J 2003;100(1):96-104.

20. Al-Mayah A, Soudki K, Plumtree A. Novel anchor system for CFRP rod: finite-element and mathematical models. J Comp for Constr 2007, ASCE;Sept/Oct:469-476.

21. Carvelli V, Fava G, Pisani MA. Anchor system for tension testing of large diameter GFRP bars. J Comp for Constr 2009, ASCE;Sept/Oct:344-349.

22. Schmidt JW, Bennitz A, Taljsten B, Pedersen H. Development of mechanical anchor for CFRP tendons using integrated sleeve. J Comp for Constr 2010, ASCE;July/August:397-405.

23. Ehsani M, Saadatmanesh H, Thompson C. Transfer and Flexural Bond Performance of Aramid and Carbon FRP Tendons. PCI J 1997;42(1):76-86.

24. Soudki KA, Green MF, Clapp FD Transfer Length of Carbon Fiber Rods in Precast Pretensioned Concrete Beams. PCI J 1997;42(5):78-87.

25. Mahmoud Z, Rizkalla SH, Zaghloul E. Transfer and Development lengths of Carbon Fiber Reinforced Polymer Prestressing Reinforcement. ACI Struct J 1999;96(4):594-602.

26. Lu Z, Boothby TE, Bakis CE, Nanni A. Transfer and Development Length of FRP Prestressing Tendons. PCI J 2000;45(2):84-95.

27. Fava G, Carvelli V, Pisani MA. Remarks on bond of GFRP rebars and concrete. Comp Part B: Eng 2016;93:210-220.

28. Yan F, Lin Z, Yang M. Bond mechanism and bond strength of GFRP bars to concrete: A review. Comp Part B: Eng 2016;98:56-69.

29. Crossett P, Taylor S, Robinson D, Sonebi M, Garcìa-Taengua E. Monitoring the transfer length of pre-stressed BFRP SCC beams. In: Proceedings of SHMII-7 Conference. Torino, July, 2015. p.10.

30. ACI 440.1R-15. Guide for the design and construction of structural concrete reinforced with fiber-reinforced polymer (FRP) bars. ACI Committee 440, Farmington Hills, MI.

31. Bischoff PH. Re-evaluation of deflection predictions for concrete beams reinforced with steel and FRP bars. J Struct Eng 2005, ASCE;131(5):752-767.

32. Zou PXW. Flexural behaviour and deformability of fiber reinforced polymer prestressed concrete beams. Constr Build Mat 2003;21:777-788.

33. Youakim SA, Karbhari VM. An approach to determine long-term behavior of concrete members prestressed with FRP tendons. Constr Build Mat 2007;27:1052-1060.

34. Zou PXW, Shang S. Time-dependent behaviour of concrete beams pretensioned by carbon fibre-reinforced polymers (CFRP) tendons. J Comp for Constr 2007, ASCE;7(4):275-284.

35. Dolan CW, Bakis CE, Nanni A. Design recommendations for concrete structures pre-stressed with FRP tendons. Report of the FHWA No. DTFH61-96-C-00019, 2001.

36. Knight D, Visintin P, Oehlers DJ. Displacement-based simulation of time-dependent behaviour of RC beams with prestressed FRP or steel tendons. Struct Concr 2016;3:406-417.

37. Pisani MA. Long-term behaviour of beams prestressed with aramid fibre cables: Part 1: a general method. Eng Struct 2000;22(12):1641-1650.

38. Pisani MA. Long-term behaviour of beams prestressed with aramid fibre cables: Part 2: an approximate solution. Eng Struct 2000;22(12):1651-1660.

39. Lou T, Lopes SMR, Lopes AV. Time-dependent behavior of concrete beams prestressed with bonded AFRP tendons. Comp Part B: Eng 2016;97:1-8.

40. Dal Lago B. Experimental and numerical assessment of the service behaviour of an innovative long-span precast roof element. Int J of Conc Struct and Mat 2017; doi:10.1007/s40069-017-0187-6.

41. Garcia-Taengua E, Sonebi M, Crossett P, Taylor S, Deegan P, Ferrara L, Pattarini A. Performance of sustainable SCC mixes with mineral additions for use in precast concrete industry. J Sust Cem-Based Mat 2016;5(3):157-175.

42. Tharmarajah G. Compressive membrane action in fibre reinforced polymer (FRP) reinforced concrete slabs. PhD thesis, University of Belfast, UK.

43. CEN-EN 1992-1-1:2005. Eurocode 2: Design of concrete structures. Part 1-1: general rules and rules for buildings. European Committee for Standardization, Brussels.

44. Ferrara L, Krelani V, Carsana M. A fracture testing based approach to assess crack healing of concrete with and without crystalline admixtures. Constr Build Mat 2014;68.

45. Ferrara L, Krelani V, Moretti F. On the use of crystalline admixtures in cement based construction materials: from porosity reducers to promoters of self healing. Smart Mat Struct 2016;25(8):084002.

46. Dal Lago B, Deegan P, Taylor S, Crossett P, Sonebi M, Ferrara L, Pattarini A. Pre-stressing using BFRP bars: an experimental investigation on a new frontier of FRSCC. In: Proceedings of CERI-7 Conference. Galway, August, 2016. p.365-370.

47. Dal Lago B, Ferrara L, Taylor S, Sonebi M, Deegan P, Kelly G, Pattarini A. Design of steel-free pre-stressed reinforced concrete slabs: theory and experimentation. In: Proceedings of the 4th ACI Italy Chapter NBSC Workshop. Capri, September, 2016. p.137-146.

48. CEB-*fib*. Model Code for Concrete Structures. Fédération Internationale du Béton / International Federation for Structural Concrete, Lausanne, 2010.

49. CEN-EN 14651:2005. Test method for metallic fibered concrete – Measuring the flexural tensile strength (limit of proportionality (LOP), residual). European Committee for Standardization, Brussels.

50. Garcia-Taengua E, Taylor S, Sonebi M, Crossett P, Deegan P, Ferrara L, Pattarini A. Effect of polypropylene macrofibers on the flexural response of SCFRC. In: Proceedings of 6th North American Conference on the Design and Use of Self-Consolidating Concrete (SCC) and 8th RILEM International Symposium on Self-Compacting Concrete (SCC), Washington DC, May, 2016. p.479-488.

51. Lydon M, Taylor S, Doherty C, Robinson D, OBrien E J, Žnidarič A. Bridge weigh-in-motion using fibre optic sensors. Proc ICE - Bridge Eng 2017; doi:10.1680/jbren.15.00033.

List of notation

A_c	area of the cross-section of concrete
A_p	total area of the pre-stressing reinforcement
A_r	area of the generic reinforcement
b	width of the horizontal cross-section chord
d	effective depth
E	Young modulus
E_{cmj}	mean Young modulus of concrete at day j
E_p	Young modulus of pre-stressing steel
$f_{p(0.1)k}$	characteristic strength of pre-stressing steel at 0.1% of residual strain
f_{pk}, f_{uk}	characteristic ultimate strength
h	depth of the cross-section
k	relaxation coefficient
I	second moment of the area
I_{id}	ideal second moment of the area of the homogenised cross-section
L	member span
L_{anch}	debonding + anchorage length of pre-stressing bar
M	bending moment
M'	maximum bending moment given by pre-stressing
M^*	maximum bending moment given by gravity loads
M_{Rd}	design resisting bending moment
N	axial load
n_p	number of pre-stressing bars
n_r	number of longitudinal reinforcing bars (either pre-stressed or non-pre-stressed)
RH	relative humidity
t	time in days
t_0	time in days from the day of release of pre-stressing
T	temperature
v	vertical deflection
v_e	elastic vertical deflection
$v_{max,p}$	maximum vertical deflection of the member under pre-stressing only
$v_{max,q+p}$	maximum vertical deflection of the member under gravity loads and pre-stressing
y	vertical position
y_g	vertical position of the centre of gravity of the cross-section
y_n	vertical position of the centre of gravity of a reinforcing bar

z_{cp}	distance between the centre of gravity of the concrete cross-section and the pre-stressing reinforcement
$\Delta\sigma_{pr}$	absolute value of the stress losses for relaxation of pre-stressing bars
ΔP_{θ}	absolute value of the load losses for accelerated hardening temperature effect
ε	strain
ε_{creep}	strain due to the viscous loss for creep
ε_{el}	strain due to the elastic loss
ε_i	initial strain
ε_{long}	longitudinal strain
ε_{cs}	total shrinkage strain of concrete
μ	relaxation coefficient
ρ_{1000}	relaxation after 1000 hours
σ	longitudinal stress
σ_p	pre-stress
σ_{p0}, σ_{pi}	initial pre-stress
φ	creep coefficient of concrete
Φ_{anch}	anchorage length correction factor
Φ_{χ}	curvature correction factor
χ	beam flexural curvature

Table 1. FRSCC mix composition.

Mix	C	GGBS	LSP	Agg. 14mm	Agg. 8mm	Sand
kg/m^3	338	113	150	215	610	825
Additives		Fibres PP	SP		SH	
kg/m^3		4	2.9		3.6	

(a)

(b)

Figure 1. Tested steel-free beam (a) cross-section and (b) void and shear truss details.

(a)   (b)   (c)   (d)

Figure 2. Tensile test setup: (a) global view, (b) particular view of the anchorage with carborundum, (c) broken bar, (d) deformed bar ends

Figure 3. Transfer length test setup
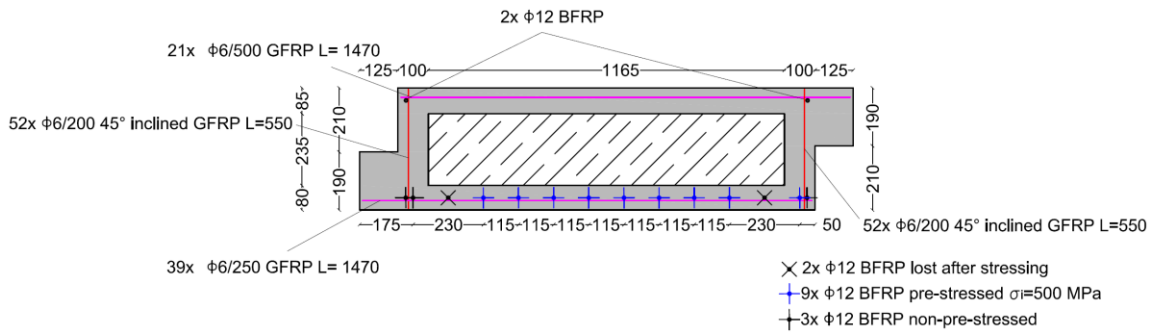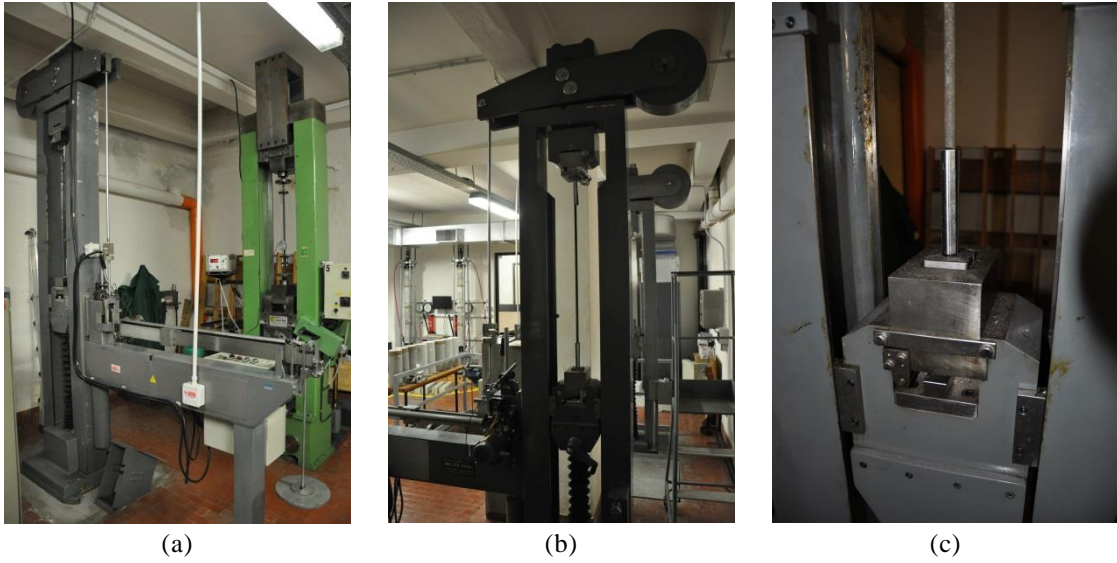
Figure 4. Pictures from the relaxation test setup: (a) test machine, (b) tensioned bar and (c) particular of the carborundum coating at anchorage
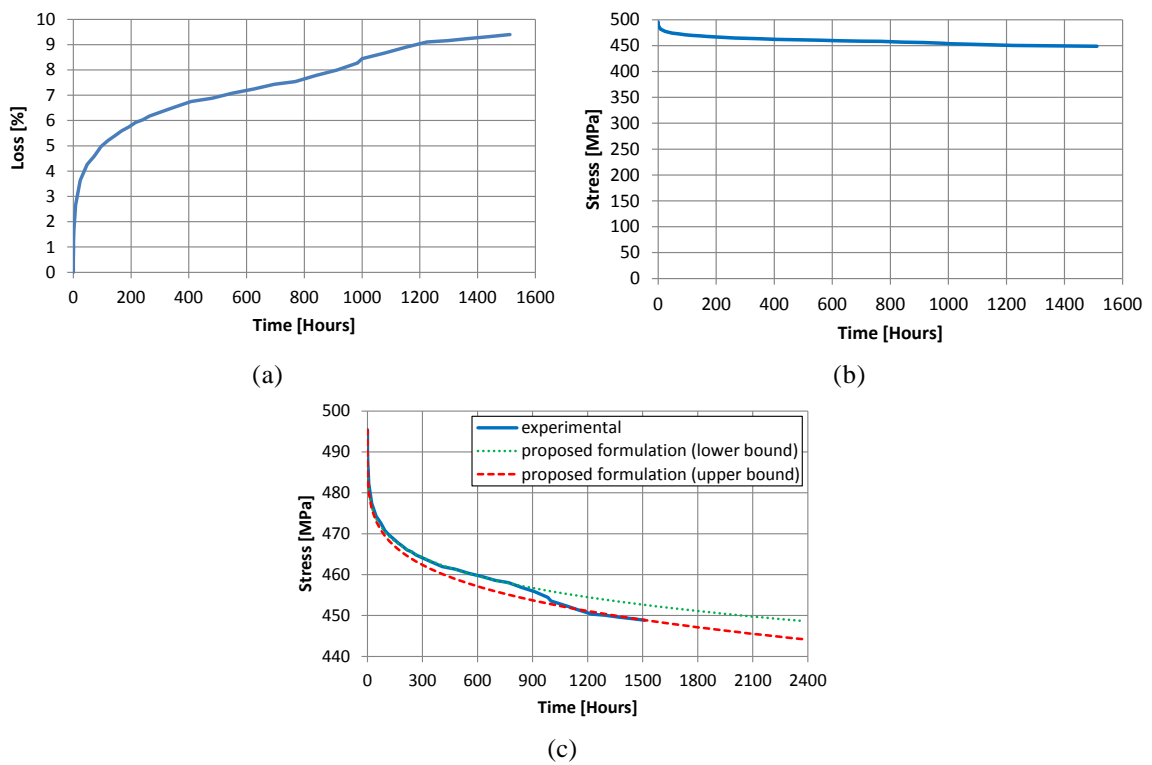

(a)

(b)

(c)

Figure 5. Relaxation test results: (a) loss percentage vs time, (b) Stress vs time and (c) comparison with the proposed formulations

(a)

(b)

(c)

(d)
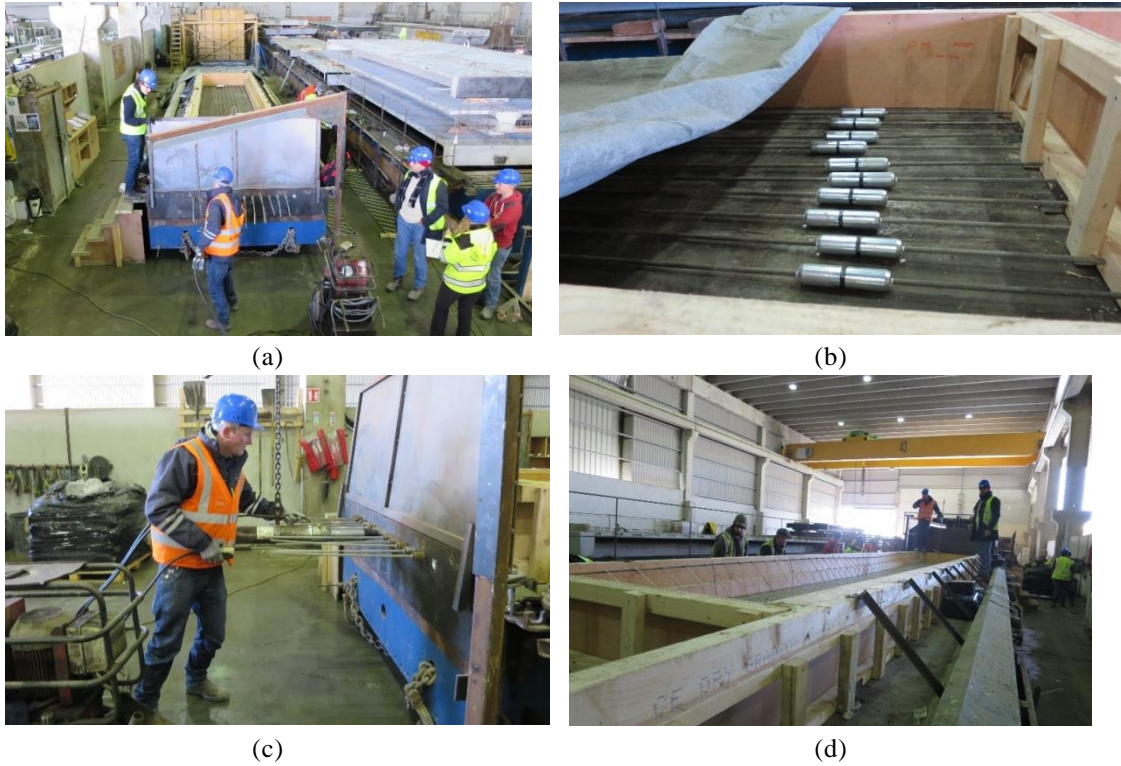
Figure 6. Manufacturing the test beam: (a) global view of the mould, (b) mechanical couplers (external to the mould), (c) tensioning operation with wedge blockage system and (d) Positioning of shear resisting trusses in correspondence of the ribs.

Figure 7. Tensile failure of one BFRP bar broken after tensioning.
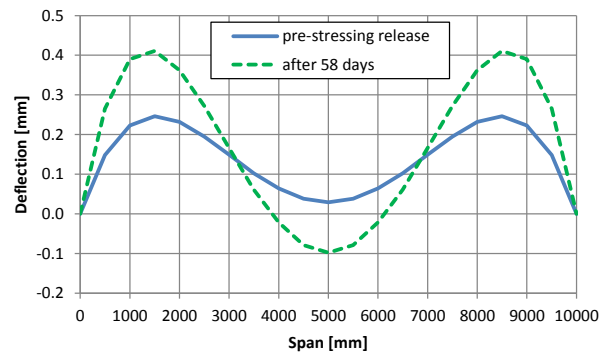
Figure 8. Deflection profile at release of pre-stressing and after 58 days.

23
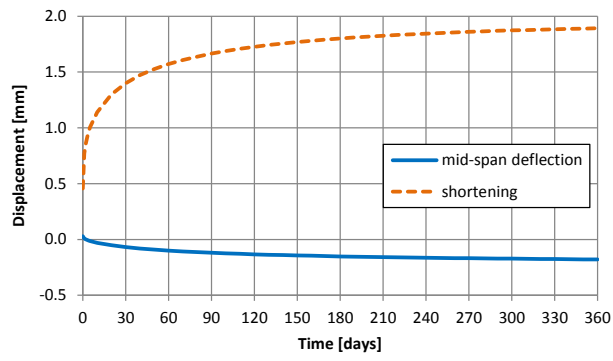
Figure 9. Predicted evolution of mid-span deflection and shortening in time.

(a)

(b)
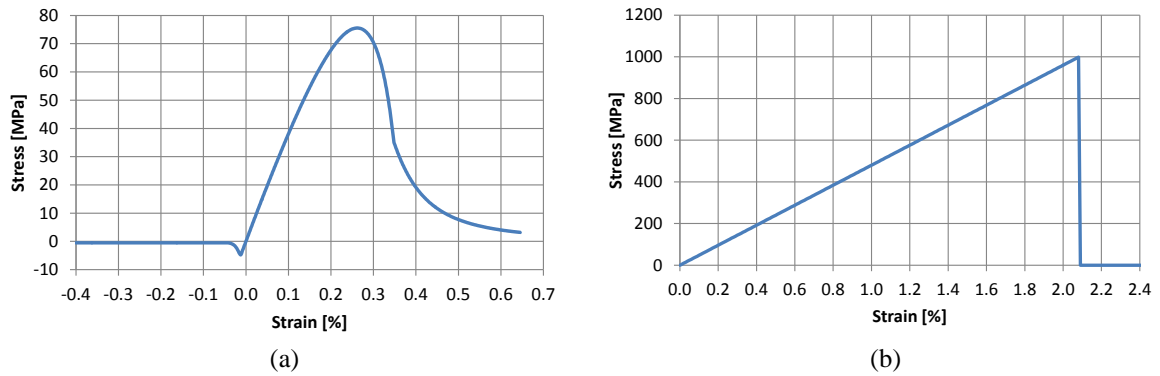
Figure 10. Material constitutive laws used in the model for (a) concrete and (b) BFRP.
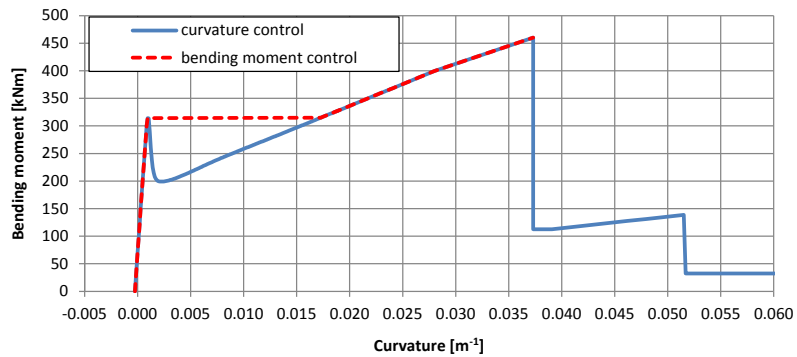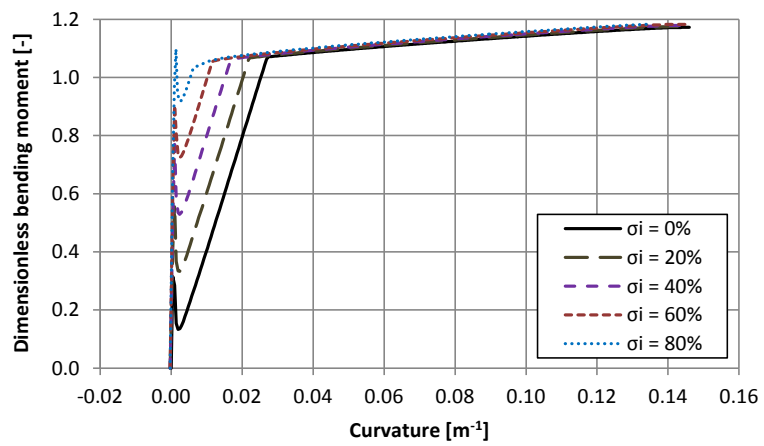

Figure 11. Non-linear bending moment vs. curvature diagrams.
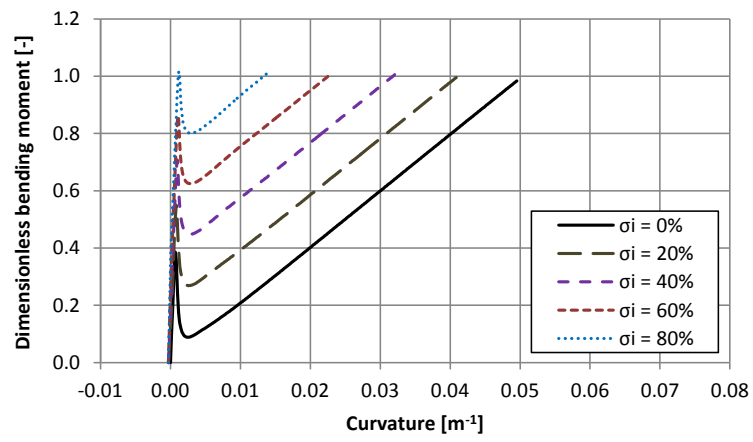
(a)

(b)

Figure 12. Non-linear dimensionless moment vs curvature diagrams with increasing pre-stressing for the investigated beam reinforced with (a) BFRP bars and (b) steel tendons.

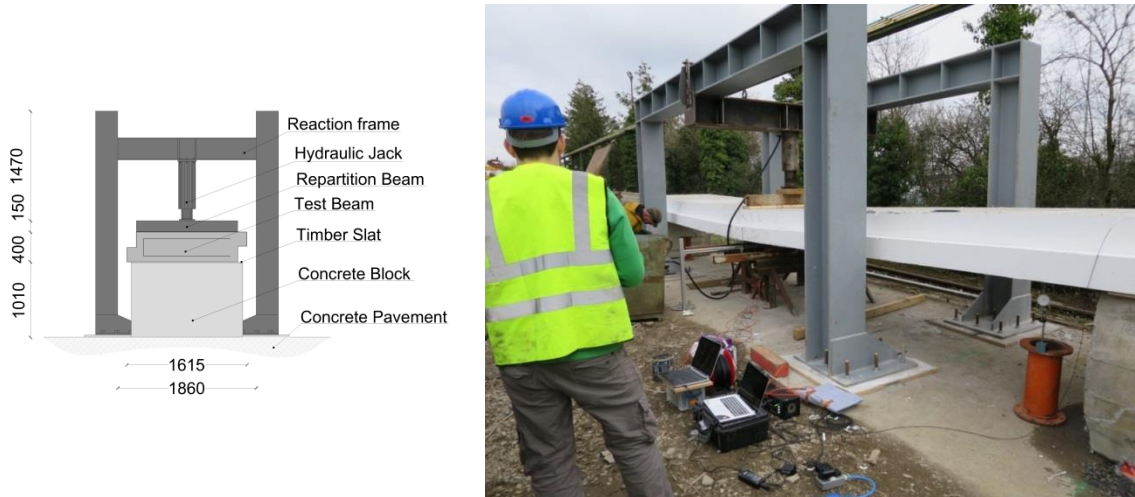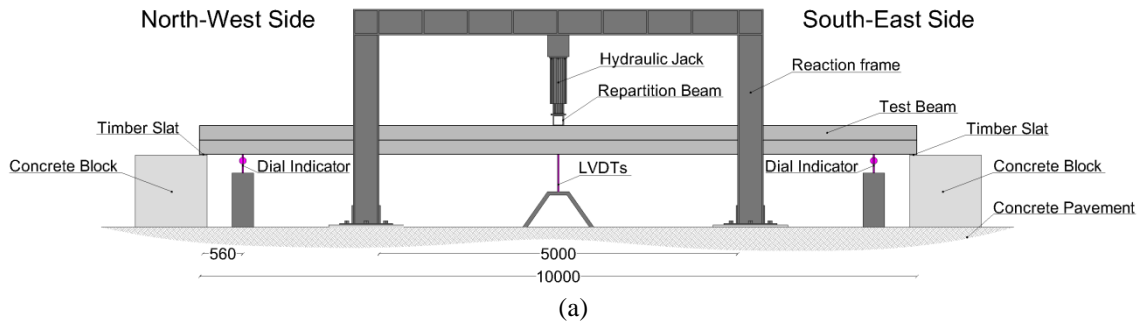Figure 13. Steel-free pre-stressed beam moving to test rig.

Figure 14. Test setup: (a) front view from South-West, (b) side view from South-East and (c) picture from South.
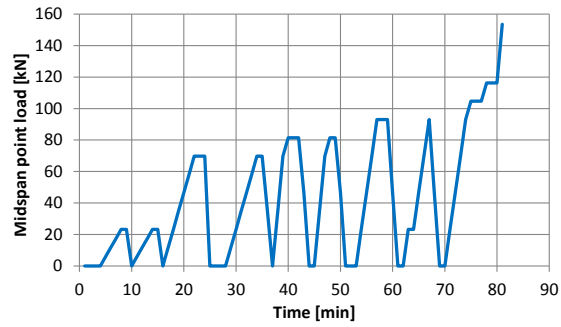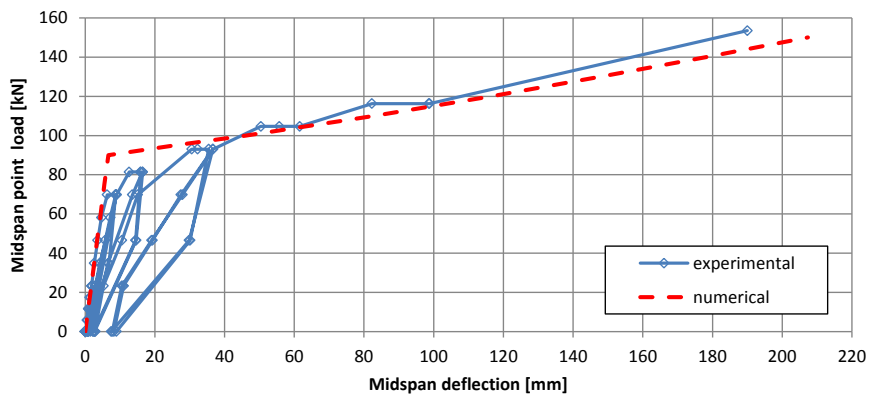

Figure 15. Load history.

26

Figure 16. Load vs deflection diagrams.

Figure 17. Test beam subject to large deflection (P = 120 kN).

Figure 18. Marked crack pattern (North-East side).

Figure 19. Crack pattern evolution with load (North-East side).

(a)   (b)

<div align="center">(c)   (d)</div>

Figure 20. Failure mode: (a) failure crack from the North-East side, (b) failure crack from the South-West side, (c) detail of broken BFRP longitudinal bar, (d) detail of intact GFRP inclined bar.